Unveiling the structure-property relationship in metastable Heusler compounds by systematic disorder tuning

F. Garmroudi, M. Parzer, M. Knopf, A. Riss, H. Michor, A. V. Ruban, T. Mori, and E. Bauer

Phys. Rev. B **107**, 014108 — Published 25 January 2023

DOI: 10.1103/PhysRevB.107.014108

Unveiling the structure – property relationship in metastable Heusler compounds by systematic disorder tuning

F. Garmroudi,[1,*] M. Parzer,[1] M. Knopf,[1] A. Riss,[1] H. Michor,[1] A. V. Ruban,[2,3] T. Mori,[4,5] and E. Bauer[1]

[1] *Institute of Solid State Physics, Technische Universität Wien, A-1040 Vienna, Austria*
[2] *Department of Materials Science and Engineering, KTH Royal Institute of Technology, SE-100 44 Stockholm, Sweden*
[3] *Materials Center Leoben Forschung GmbH, A-8700 Leoben, Austria*
[4] *International Center for Materials Nanoarchitectonics (WPI-MANA), National Institute for Materials Science, Tsukuba 305-0044, Japan*
[5] *University of Tsukuba, Tsukuba 305-8577, Japan*

Heusler compounds represent a unique class of materials that exhibit a wide range of fascinating and tuneable properties such as exotic magnetic phases, superconductivity, band topology or thermoelectricity. An exceptional, but for Heusler compounds common feature is that they are prone to antisite defects and disorder. In this regard, the Fe_2VAl Heusler compound has been a particularly interesting and disputed candidate. Even though, various theoretical scenarios for the interplay of physical properties and disorder have been proposed, the metastable disordered A2 phase hitherto precluded experimental investigation in bulk samples. Here, we report experimental results on disorder-tuned $Fe_2VAl_{0.9}Si_{0.1}$ alloys all the way towards the A2 phase, which we realized via rapidly quenching our samples from high temperatures. We measured the thermoelectric properties of these materials in a wide temperature range (4 to 700 K), which suggest a gradual semimetal/narrow-gap semiconductor $\rightarrow$ metal transition upon increasing the disorder. We also find a large anomalous Hall effect in the disordered A2 phase, arising from the side-jump scattering of charge carriers at the antisite magnetic moments. This is corroborated by measurements of the temperature- and field-dependent magnetization, which increases dramatically up to $\approx 2.5\,\mu_B$/f.u. as compared to the ordered compound ($< 0.1\,\mu_B$/f.u.). This study provides the first experimental realization of the metastable A2 structure in bulk Fe_2VAl-based alloys and grants insight into the structure – property relationship of these materials. Our work confirms that temperature-induced antisite disorder, occuring during thermal heat treatment, can be a precisely tuneable parameter in the family of Heusler compounds.

Keywords: Heusler; disorder; thermodynamic; thermoelectric; transport; magnetism; anomalous Hall effect

I. INTRODUCTION

Over a century ago, Friedrich Heusler made the remarkable discovery that, despite consisting of non-magnetic elements, Cu_2MnAl exhibits long-range ferromagnetic order [1, 2]. Today, Heusler compounds comprise a vast group of more than a thousand members that can be categorized into so-called half-Heuslers with the nominal composition XYZ and full-Heuslers (X_2YZ) [3]. Since their crystal structure can host a large variety of different elements from the periodic table, these compounds have shown to exhibit a wide range of physical phenomena, making them ideal materials for both fundamental and applied research [4–8].

Within the family of Heusler compounds, structural defects are ubiquitous. It has long been reported that half-Heusler compounds such as RNiSn (R = Ti, Zr, Hf) are prone to antisite defects due to the close structural relationship between the half-Heusler and full-Heusler phase [9–12]. These half-Heusler systems are also highly efficient thermoelectric materials with excellent properties [13] and it was shown that disorder can have a significant impact on the thermoelectric transport behavior [14, 15] as it affects the scattering of electrons and phonons. It was also shown that structural instabilities, point defects, or natural off-stoichiometry in half-Heuslers can lead to drastic changes in the electronic structure and doping behavior [16–18]. However, antisite disorder can occur also in other Heusler compounds, such as full-Heuslers [19, 20] as well as quaternary Heuslers [21], severely influencing the magnetic and electronic properties of these materials.

Amongst these Heusler systems, Fe_2VAl has attracted great interest, not only due to its peculiar physical properties [22–26], but also, for instance, with respect to thermoelectric applications [27–35]. Fe_2VAl obeys the Slater-Pauling rule [36–39] of Heusler compounds and is a semimetal/narrow-gap semiconductor (the absolute size of the gap remains a subject for discussion) [40–42] with a non-magnetic groundstate. However, it was shown that the ordered $L2_1$ crystal structure in these compounds undergoes certain order – disorder transitions driven by temperature or mechanical stress [43]. For partial disorder between the V and Al sublattices, the crystal structure reduces to a simple *bcc* B2 structure (CsCl-type). When all sublattices are fully disordered, a further simplification to the tungsten-type A2 structure occurs (see Fig. 1a). A recent study reported that the metastable A2

* fabian.garmroudi@tuwien.ac.at

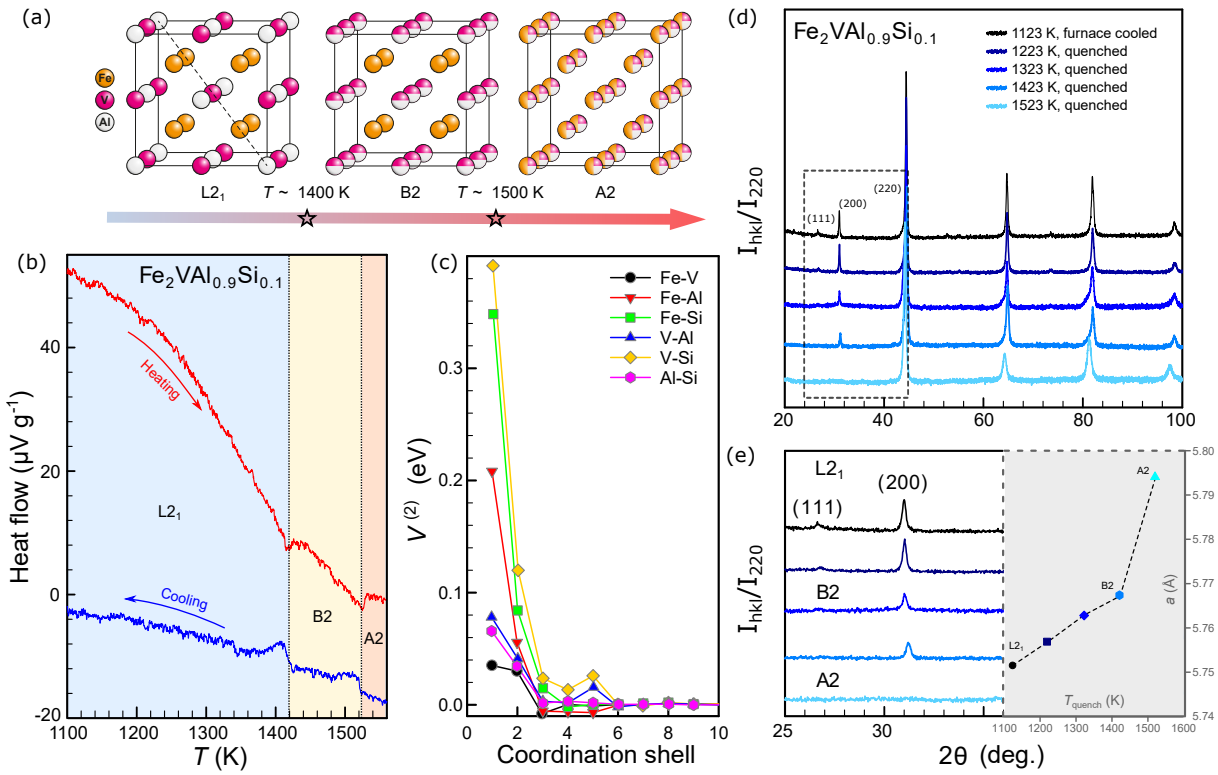

FIG. 1. (a) Order – disorder transitions in Fe_2VAl from the fully ordered $L2_1$ phase in to the partly disordered B2 and fully disordered A2 phase, occuring at high temperatures. (b) Differential thermal analysis (DTA) of $Fe_2VAl_{0.9}Si_{0.1}$ upon heating and cooling. (c) Effective pair interactions in a random *bcc* $Fe_{0.5}V_{0.25}Al_{0.225}Si_{0.025}$ alloy at $T = 1500\,K$ from *ab initio* thermodynamics simulations. (d) X-ray powder diffraction (XRD) patterns of disorder-tuned $Fe_2VAl_{0.9}Si_{0.1}$ Heusler compounds. (e) XRD patterns near the (111) and (200) Bragg positions, showcasing the order – disorder transitions into the B2 and A2 phases in our samples. Inset shows the lattice parameter for the different samples.

structure, stabilized in $Fe_2V_{0.8}W_{0.2}Al$ thin films, could be responsible for the record-high thermoelectric performance measured in these films [30]. On the other hand, bandstructure calculations by Alleno *et al.* have not revealed promising features of the electronic density of states (eDOS) near the Fermi energy E_F, which would originate large values of the Seebeck coefficient [44]. Matsuura *et al.* proposed instead a huge magnon drag thermopower in these Heusler alloys as a possible explanation for the observed enhancement [45]. Furthermore, two recent theoretical studies argued that V-Al antisite exchange defects in Fe_2VAl can result in an unexpected band gap opening [46, 47], therefore significantly increasing the Seebeck coefficient [47]. This, however, is not in agreement with our recent work, which showed that increasing the lattice disorder by thermal quenching in stoichiometric Fe_2VAl leads to an Anderson-type insulator – metal transition [48]. However, so far, high levels of disorder and the metastable A2 structure could not be experimentally investigated in bulk samples due to the short time scale of the ordering into the B2 structure.

Here, we show for the first time that the lattice disorder can be tuned in the whole disorder range towards the A2 structure in Si-substituded $Fe_2VAl_{0.9}Si_{0.1}$ by rapid quenching, allowing experimental investigations with respect to the electronic transport and magnetic properties. In the following, theoretical results from *ab initio* thermodynamics calculations, experimental results of structural analysis by X-ray powder diffraction (XRD) as well as differential thermal analysis (DTA), temperature-dependent measurements of the electrical resistivity and Seebeck coefficient in a wide temperature range (4 to 700 K) as well as temperature- and field-dependent measurements of the magnetization and Hall resistivity are presented. Comprehensive multi-band models allow us to discuss phenomenologically the evolution of electronic transport properties upon increasing disorder.

II. EXPERIMENTAL AND COMPUTATIONAL METHODS

Highly pure bulk elements (Fe 99.99 %, V 99.93 %, Al 99.999 %, Si 99.9999 %) were stoichiometrically weighed to a nominal composition $Fe_2VAl_{0.9}Si_{0.1}$ and melted in a high-frequency induction furnace under argon atmosphere. The mass loss for the polycrystalline sample (mass of $\approx 5\,g$) was around 0.1 %, even after remelting

the ingot several times. The as-cast ingot was sealed in a quartz tube at approximately 10^{-5} mbar and subjected to heat treatment for homogenization for 7 days, followed by furnace cooling. The annealing temperature was set to 1123 K, sufficiently below the B2 order – disorder transition found in Ref. [43]. Thereafter, the annealed ingot was cut into five rectangular pieces. Four of the fives pieces were subjected to further heat treatment at 1223, 1323, 1423 and 1523 K, respectively, while the duration of the additional heat treatment was reduced to 48 h. The quartz tubes were filled with argon to ensure thermal conductance to the water bath during the quenching procedure.

The crystal structure of each sample was probed by X-ray powder diffraction in a Bragg-Brentano geometry using Cu-Kα radiation. Measurements were carried out at the X-ray center, TU Wien. For the high-temperature ($>$ 300 K) resistivity and Seebeck coefficient measurements, a commercially available setup (ULVAC-ZEM3) was used. Low-temperature resistivity was measured in our in-house setup, using a four-probe method and employing a LAKESHORE a.c. resistance bridge. To this aim, thin gold wires were spot-welded onto the sample surface and the sample was mounted on a sample holder, which was immersed in a liquid helium bath cryostate. The Seebeck coefficient from $4 - 300$ K was measured making use of chromel constantan thermocouples and a toggled heating technique to cancel spurious voltages. Temperature- and field-dependent measurements of the d.c. magnetisation were performed in a superconducting quantum interference device (CRYOGENIC). To obtain the Hall effect, the van der Pauw method was used. Therefore, we cut thin ($0.2 - 0.3$ mm) disk-shaped pieces from our samples which were contacted with thin gold wires in the appropriate geometry.

In order to further investigate the effect of Si substitution in the $Fe_2VAl_{0.9}Si_{0.1}$ Heusler compound on the order – disorder transition temperatures, we also performed statistical thermodynamics simulations in the framework of the screened generalized perturbation method (SGPM) [49, 50] within the Lyngby version of the exact muffin tin orbital coherent potential approximation (EMTO-CPA) code [51]. The configurational Hamiltonian for the calculations is given by:

$$H = \frac{1}{2}\sum_{p}\sum_{\alpha,\beta\neq\delta} V_p^{(2)-\alpha\beta[\delta]} \sum_{i,j\in p} \delta c_i^{\alpha}\delta c_j^{\beta} + \frac{1}{3}\sum_{t}\sum_{\alpha,\beta,\gamma\neq\delta} V_t^{(3)-\alpha\beta\gamma[\delta]} \sum_{i,j,k} \delta c_i^{\alpha}\delta c_j^{\beta}\delta c_k^{\gamma} + \text{h.o.t.} \quad (1)$$

Summations are performed over different types of clusters (p and t are the indices of pairs and triangles), alloy components are designated by Greek letters and lattice sites have the indices i, j and k. $V_p^{(2)-\alpha\beta[\delta]}$ and $V_t^{(3)-\alpha\beta\gamma[\delta]}$ are the pair- and three-site effective interactions. The same types of calculations were performed recently to understand the order – disorder behavior at high temperatures in stoichiometric Fe_2VAl [48]. Likewise to our previous study, strain-induced interactions related to the local lattice relaxations from the sized mismatch of the alloy components as well as lattice vibrations have been neglected since these contributions are computationally very expansive for multicomponent alloys and outside the scope of this work. Clearly, both these effects, thermal lattice vibrations and local lattice relaxations, affect mostly the first B2 – A2 order – disorder transition, not the second $L2_1$ – B2 one, since both of them are mainly related to the interactions at the first coordination shell. However, as the atomic mass and size of Si and Al is very similar, these missing effects are probably similar for Si-substituted and pristine Fe_2VAl, allowing a qualitative comparison of the order – disorder transitions in $Fe_2VAl_{0.9}Si_{0.1}$ and stoichiometric Fe_2VAl. Further computational details on the modelling procedure can be found in the methods section of Ref. [48].

III. RESULTS

A. Crystal structure

The Fe_2VAl Heusler compound has long been known to be susceptible to the formation of antisite defects on all sublattices [25, 43, 52–59]. This also manifests itself in the high solubility and chemical stability of Fe, V, and Al on the other sublattices within a large range of off-stoichiometric compositions. For instance, the Fe content in $Fe_{2+x}V_{1-x}Al$ can be tuned in the whole range from $-2 \leq x \leq 1$ [60, 61]. Moreover, recently it could be shown that Al in off-stoichiometric $Fe_2VAl_{1+\delta}$ can be hosted in the crystal structure as antisites on Fe and V sites ($Fe_{2-2x}V_{1-x}Al_{1+3x}$) all the way up to Fe_2VAl_2 [33]. In the stoichiometric Fe_2VAl compound, antisite defects naturally occur during heat treatment or synthesis [43, 48, 59].

Fig. 1a sketches the order – disorder transition from the fully ordered $L2_1$ phase into the partly disordered B2 phase and fully disordered A2 phase. Fig. 1b shows temperature-dependent differential thermal analysis (DTA) up to $\approx$ 1560 K. Heating and cooling curves show two endothermic and two exothermic peaks, respectively. These peaks occur at temperatures which are more or less consistent with those found for pristine Fe_2VAl by Maier et al. [43]. This means that the B2- and A2- order – disorder transitions in $Fe_2VAl_{0.9}Si_{0.1}$ occur roughly at the same temperature as in undoped Fe_2VAl. This is corroborated by our statistical Monte Carlo simulations, yielding a lowering of the transition temperature into the A2 phase by about only 30 K, whereas even an increase of $\approx$ 130 K is predicted for the $L2_1$ – B2 transition. Fig. 1b shows the effective pair interactions in the *bcc* random alloy at 1500 K. The strongest pair effective interactions are calculated for Fe-Si and V-Si pairs at the first coordination shell, which are almost twice as large

as the Fe-Al interaction. Similar to the pair interactions, the substitution of Al/Si leads to the appearance of very strong three-site and four-site interactions.

In order to experimentally investigate the high-temperature metastable phases of this Heusler compound, we systematically tuned the number of antisite defects in a single $Fe_2VAl_{0.9}Si_{0.1}$ bulk sample by thermal quenching (details see Methods). Figs. 1d,e show the XRD patterns of $Fe_2VAl_{0.9}Si_{0.1}$ samples after applying different heat treatment conditions. It can be seen in Fig. 1d that the (111) and (200) Bragg peaks, associated with B2-type and A2-type disorder, respectively, gradually vanish when increasing the quenching temperature. Indeed, the furnace-cooled sample exhibits both peaks, although the intensity of the (111) Bragg peak at 27 degrees is diminished as a result of hand grinding as discussed in Refs. [43, 59]. Above a quenching temperature of 1423 K, the (111) peak can no longer be observed, which is in agreement with our DTA curves and also with *in situ* neutron diffraction studies at high temperatures by Maier *et al.* on stoichiometric Fe_2VAl [43]. For the 1523 K-quenched sample, both (111) and (200) Bragg peaks are absent, confirming the tungsten-type A2 structure in this sample. Again, this is in agreement with our DTA results as well as with the B2 – A2 transition temperature obtained by Maier *et al.* [43] and by van der Rest *et al.* [59], who performed neutron diffraction as well as specific heat measurements on stoichiometric Fe_2VAl samples. Interestingly, while the metastable A2 structure in undoped Fe_2VAl could not be stabilized by thermal quenching so far, neither by the authors of Ref. [59] nor in our recent study [48], we realized A2-$Fe_2VAl_{0.9}Si_{0.1}$ in this work, despite the small changes in the transition temperatures compared to the stoichiometric Fe_2VAl compound. While our *ab initio* thermodynamics simulations suggest that the B2 – A2 order – disorder transition is only slightly lowered, this effect is probably too small to explain the much larger degree of disorder in quenched $Fe_2VAl_{0.9}Si_{0.1}$ samples compared to Fe_2VAl as evidenced by our XRD results. Thus, it is likely that the substitution of Al/Si changes significantly the diffusion kinetics and time-scale of the order – disorder transitions in this Heusler system. Usually, the major driving mechanism for diffusion in metals and alloys are thermal vacancies induced by the configurational entropy at high temperatures. We estimated the binding energy of thermal vacancies with Fe, V, Al and Si atoms using the SGPM method and found that the strongest repulsion among all the atom – vacancy pairs is for V and the vacancy at both coordination shells (about −1.0 and −0.2 eV respectively), while the weakest repulsion at the first coordination shell is for the Si – vacancy pair, −0.46 eV. Moreover, the Si-vacancy interactions become strongly attractive at the second coordination shell: about 0.42 eV. This is an extremely strong interaction. Thus, thermal vacancies may indeed be bound towards Si atoms in the disordered alloy, which hinders diffusion and slows down the ordering process during the quenching procedure, allowing us to investigate higher degrees of atomic disorder in these Heusler systems.

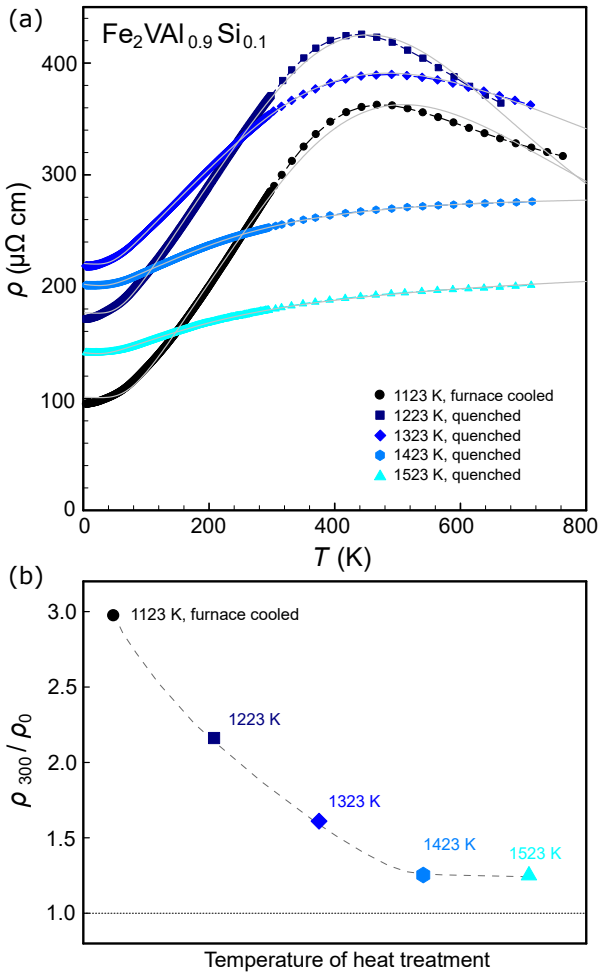

FIG. 2. (a) Temperature-dependent electrical resistivity and (b) residual resistivity ratio of disorder-tuned $Fe_2VAl_{0.9}Si_{0.1}$ Heusler compounds. Solid lines are guides to the eye.

The effect of increasing disorder in our samples also manifests itself in a substantial increase of the room-temperature lattice parameter, which increases from $a \approx 5.75$ Å in furnace-cooled $Fe_2VAl_{0.9}Si_{0.1}$ up to $a^* \approx 5.80$ Å in the fully disordered A2 phase (see inset Fig. 1e). It should be noted that, due to the change in the crystal symmetry from *fcc* to *bcc*, the lattice parameter of the *bcc* unit cell in the A2 phase is technically given by $a = \frac{a^*}{2}$.

B. Electrical resistivity

Figs. 2a,b show the temperature-dependent electrical resistivity $\rho(T)$ as well as the sample-dependent residual resistivity ratio (RRR) ρ_{300}/ρ_0. Here, ρ_{300} denotes the resistivity at 300 K and ρ_0 the residual resistivity. Fig. 2a shows that $Fe_2VAl_{0.9}Si_{0.1}$ samples quenched at temperatures up to a critical quenching temperature $T_{\mathrm{quench}} \approx$

1323 K exhibit a pronounced maximum in their resistivity curve above room temperature, which can be associated with the pseudogap/band gap close to the Fermi energy E_F [27, 62, 63]. Indeed, it was shown in several studies that Al/Si substitution in Fe_2VAl shifts the chemical potential from within the gap region into the conduction band, yielding metallic behavior, $d\rho/dT > 0$, at low temperatures [27, 64, 65]. However, when k_BT is large enough, charge carriers get excited across the gap, resulting in semiconductor-like behavior, $d\rho/dT < 0$, at high temperatures. As we demonstrated in a recent study, the Hall carrier concentration indeed also increases rapidly at $T \approx 450$ K, where the resistivity maximum occurs [31].

This semimetallic trend is no longer observable for disordered samples quenched from higher temperatures $T_{quench} = 1423$, 1523 K. Instead, the metallic behavior persists at least up to 700 K – although a slightly saturating behavior is noticeable.

Furthermore, the residual resistivity ρ_0 first increases up to a quenching temperature of $T_{quench} = 1323$ K but then gradually decreases when further increasing the disorder. This can be understood from the interplay of charge carrier concentration, which increases due to the occurence of in-gap impurity states [48], as well as a reduction of carrier mobility caused by the lattice disorder and point defect scattering. The A2-type disorder, which is the main reason for the formation of in-gap defect states [48, 57, 66], becomes increasingly relevant towards higher quenching temperatures [43, 48]. Thus, the increased scattering rate and mobility reduction due to B2-type disorder first dominates the evolution of $\rho(T)$ at lower T_{quench} until it gets superseded by the increase of the carrier concentration.

Another obvious trend which can be observed is the flattening of temperature-dependent resistivity curves. While acoustic phonon scattering dominates the resistivity of structurally ordered $Fe_2VAl_{0.9}Si_{0.1}$, the scattering off random potential fluctuations caused by the point defects and disorder monotonically increases with T_{quench}. Fig. 2b shows the RRR for all samples. With elevating quenching temperature, the RRR decreases, approaching values close to $\rho_{300}/\rho_0 = 1$, which confirms that the lattice disorder increases and can be readily tuned by thermal quenching.

C. Seebeck coefficient

The temperature-dependent Seebeck coefficient $S(T)$ of disorder-tuned $Fe_2VAl_{0.9}Si_{0.1}$ is shown in Fig. 3. Since $Fe_2VAl_{0.9}Si_{0.1}$ is a semimetal with a large gradient of the density of states near E_F, the Seebeck coefficient shows sizeable negative values, signalizing electrons as the principal charge carriers. Upon increasing the lattice disorder in $Fe_2VAl_{0.9}Si_{0.1}$, $S(T)$ monotonically decreases in absolute values, yielding only small metallic Seebeck coefficients $|S| < 10\,\mu$V/K for B2- and A2-$Fe_2VAl_{0.9}Si_{0.1}$. We note that in stoichiometric Fe_2VAl, on the contrary,

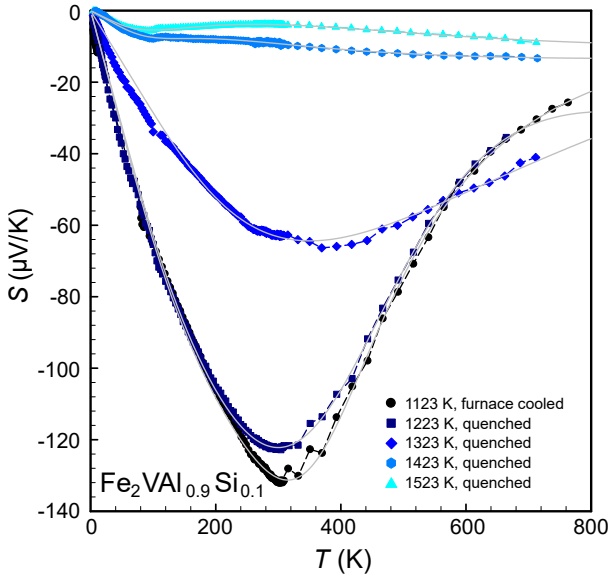

FIG. 3. Temperature-dependent Seebeck coefficient of disorder-tuned $Fe_2VAl_{0.9}Si_{0.1}$ Heusler compounds. Solid lines are least-squares fits employing a triple parabolic band model as explained in the text (further modelling details see Ref. [31]).

the disorder tuning led to an enhancement of thermoelectric properties, which we ascribed to a delocalized impurity band at the Fermi energy [48]. For Si-substituted $Fe_2VAl_{0.9}Si_{0.1}$, $|S(T)|$ gradually deteriorates which could be explained from a different position of E_F relative to the undoped Fe_2VAl compound. Another possibility could be that the emergent impurity states caused by disorder appear at slightly different energies compared to the undoped Fe_2VAl compound. We point out that we observed low-temperature anomalies in the temperature-dependent Seebeck coefficient of heavily disordered B2- and A2-$Fe_2VAl_{0.9}Si_{0.1}$, which might be attributed to remnants of impurity bands leading to additional features in the energy-dependent eDOS, as will be discussed in section IV.

D. Magnetization

The magnetization of two selected samples, one in the low-disorder limit (furnace cooled) as well as A2-$Fe_2VAl_{0.9}Si_{0.1}$, was measured as a function of magnetic field and temperature. Fig. 4a shows the field-dependent behavior of the low-temperature magnetization at $T = 4$ K. We also compare our results with those obtained recently for stoichiometric undoped Fe_2VAl [48]. In Fe_2VAl-based Heusler compounds, the magnetic properties can be significantly altered in the presence of antisite disorder. For instance, while Fe atoms occupying the Fe sublattice show no magnetic moment, a large magnetic moment appears when the V or Al sublattices are occupied by Fe antisite defects [48, 52, 57, 66]. It can be

seen in Fig. 4a that the magnetization quickly saturates and the saturation magnetization $M_{\rm sat}$ significantly increases for the high-temperature quenched samples, reflecting the higher degree of antisite disorder. For the Si-substituted sample $M_{\rm sat} \approx 2.5\,\mu_{\rm B}$/f.u. is almost three times larger than for stoichiometric Fe_2VAl, as expected from the larger amount of antisite disorder, evidenced by the X-ray diffraction in this work. Thus, while the substitution of Al/Si increases the accessible phase space of antisite disorder by thermal quenching in Fe_2VAl-based Heusler compounds.

Moreover, we find no hysteresis in the isothermal magnetization curves. We note that recent experimental studies on full-Heusler-type $Fe_2V_{0.9}Cr_{0.1}Al_{0.9}Si_{0.1}$ and $Fe_{2.2}V_{0.8}Al_{0.6}Si_{0.4}$ showed very similar behaviors which were identified as weak itinerant ferromagnets [67]. However, the saturation magnetization of A2-$Fe_2VAl_{0.9}Si_{0.1}$ is quite high. It is likely that the absence of hysteresis, the lack of a transition temperature but simultaneously high magnetization are a result of the structural disorder, resembling the properties of glassy and amorphous magnetic materials.

E. Anomalous Hall effect

The Hall effect was measured for the low-disorder ($L2_1$-$Fe_2VAl_{0.9}Si_{0.1}$) and high-disorder samples (A2-$Fe_2VAl_{0.9}Si_{0.1}$), to directly compare the effect of antisite disorder and further characterize the transport properties of metastable A2-$Fe_2VAl_{0.9}Si_{0.1}$. Fig. 5 shows the isothermal Hall resistivity ρ_{xy} as a function of the magnetic field for different temperatures. It can be immediately observed that the disordered $Fe_2VAl_{0.9}Si_{0.1}$ sample quenched from high temperatures, displays an anomalous contribution to the Hall effect. Usually, the Hall resistivity can be separated into a normal contribution, arising from the Lorentz force acting on charge carriers in the presence of an applied magnetic field and an anomalous contribution: $\rho_{xy} = R_{\rm H}\,B + (\alpha\rho_{xx}^2 + \beta\rho_{xx})M$. Here, $R_{\rm H}$ denotes the Hall coefficient and ρ_{xx} and M the longitudinal resistivity and magnetization, respectively. The parameter α is dictated by the intrinsic Berry curvature and extrinsic side-jump scattering and β stems from skew-scattering effects [8]. The anomalous Hall resistivity $\rho_{xy,\rm A}$ in our sample is about $3-4$ times smaller than $\rho_{xy,\rm A}$ reported previously in weakly ferromagnetic $Fe_2V_{0.9}Cr_{0.1}Al_{0.9}Si_{0.1}$ Heusler compounds [67]. However, $\rho_{xy,\rm A}$ is about twice as large compared to the AHE observed in ferromagnetic $Fe_{1-x}Co_xSi$ semiconductors [68]. The anomalous contribution increases with temperature and reflects the magnetic behavior of these materials, arising from the antisite disorder. We also calculated the Hall conductivity defined as $\sigma_{xy} = \rho_{xy}/(\rho_{xy}^2 + \rho_{xx}^2)$, resulting in $\sigma_{xy} \approx 100 - 120\,(\Omega\,{\rm cm})^{-1}$ for A2-$Fe_2VAl_{0.9}Si_{0.1}$, which are typical values for magnets with similar magnetization [68].

To gain further insight into the electronic transport

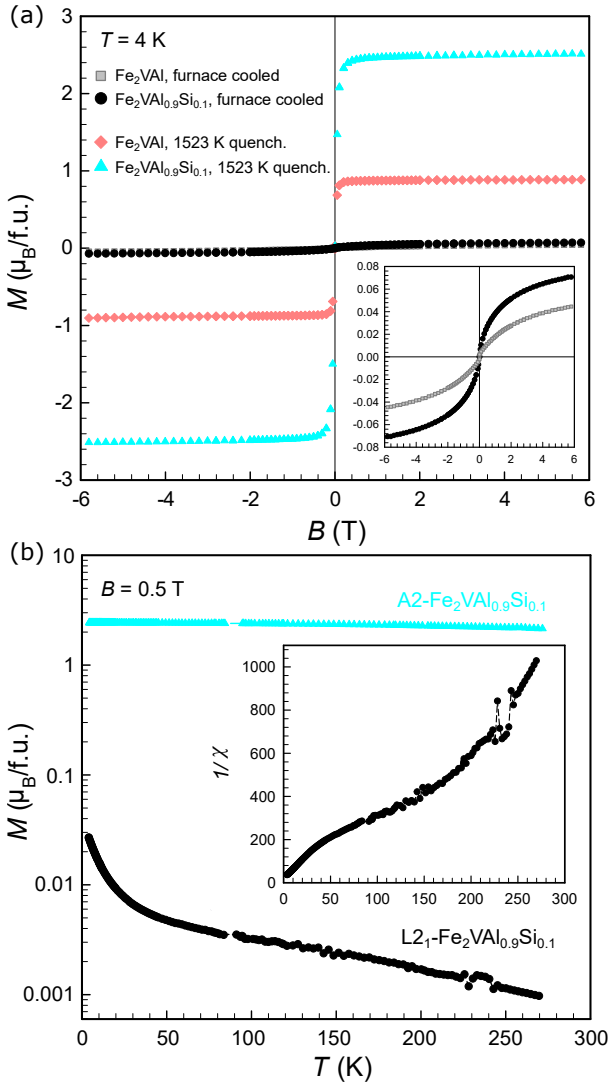

FIG. 4. (a) Isothermal magnetization as a function of the magnetic field at $T = 4\,$K. We compare ordered ($L2_1$) and fully disordered (A2) $Fe_2VAl_{0.9}Si_{0.1}$ Heusler compounds as well as stoichiometric undoped Fe_2VAl under the same heat treatment conditions. Inset shows a magnification of the field-dependent behavior for the ordered compounds. (b) Temperature-dependent magnetization of ordered ($L2_1$) and fully disordered (A2) $Fe_2VAl_{0.9}Si_{0.1}$. Inset shows the inverse temperature-dependent magnetic susceptibility for the ordered compound.

properties of disorder-tuned $Fe_2VAl_{0.9}Si_{0.1}$ Heusler compounds, we extracted the Hall mobility $\mu_{\rm H} = (\rho_{xx}R_{\rm H})^{-1}$ and carrier concentration $n_{\rm H} = (eR_{\rm H})^{-1}$ of $L2_1$- and A2-$Fe_2VAl_{0.9}Si_{0.1}$ at $T = 4\,$K. While the Hall carrier concentration of ordered $Fe_2VAl_{0.9}Si_{0.1}$ is of the order of $n_{\rm H} \approx 1.4 \cdot 10^{21}\,{\rm cm}^{-3}$, disordered A2-$Fe_2VAl_{0.9}Si_{0.1}$ has a carrier concentration which is more than an order of magnitude larger ($n_{\rm H} \approx 1.8 \cdot 10^{22}\,{\rm cm}^{-3}$). Similarly, the Hall mobility also changes dramatically. The ordered compound shows mobilities around $\mu_{\rm H} \approx 47\,{\rm cm}^2{\rm V}^{-1}{\rm s}^{-1}$ and the Hall mobility of $Fe_2VAl_{0.9}Si_{0.1}$ in its disordered

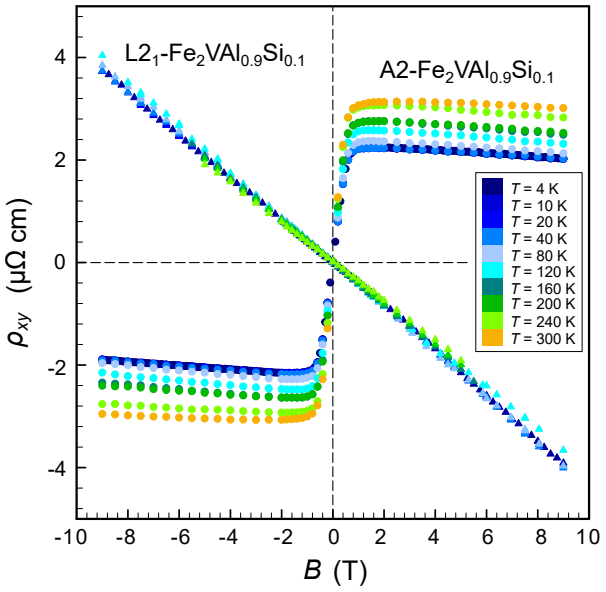

FIG. 5. Isothermal Hall resistivity as a function of the magnetic field at different temperatures. We compare ordered ($L2_1$) and fully disordered (A2) $Fe_2VAl_{0.9}Si_{0.1}$ Heusler compounds. For the latter, an anomalous Hall effect, which increases with temperature, can be observed.

A2-phase is only $\mu_H \approx 2-3\,\mathrm{cm^2V^{-1}s^{-1}}$. These results are in agreement with the overall evolution of the Seebeck coefficient and electrical resistivity in disorder-tuned $Fe_2VAl_{0.9}Si_{0.1}$.

IV. DISCUSSION

A. Effective band gap from temperature-dependent Seebeck data

The semimetal/narrow-gap semiconductor → metal transition with increasing antisite disorder in Fe_2VAl is driven by the occurence of spin-polarized impurity states inside the band gap [48]. However, at smaller concentration of defects, these impurity states are localized due to combined effects of Anderson and Mott localization. Thus, at the low disorder level, these in-gap states do not contribute to the electrical resistivity and Seebeck coefficient themselves by band-like transport. Only above a critical concentration, electrons become delocalized and can significantly contribute to the overall charge transport. Since the incorporation of impurity bands for spin-up and spin-down electrons in addition to the pristine bandstructure, which already shows many complex features, would require numerous fitting parameters in our transport model, we focus on a more qualitative and simpler analysis in terms of three bands with parabolic dispersion $E(k) \sim k^2$. This way, $S(T)$ of a single conduction channel (electronic band) can be written in the Fermi integral formalism as

$$S(T) = \frac{k_B}{e}\left[\frac{(\lambda+2)F_{1+\lambda}(\eta,T)}{(\lambda+1)F_\lambda(\eta,T)} - \eta\right], \qquad (2)$$

with η being the reduced chemical potential, F_n being the Fermi integrals of nth order and $\lambda = 0$ for dominant acoustic phonon scattering. The total Seebeck coefficient is then given by weighting the single-band contributions with the electrical conductivities $S_{tot} = \sum_i S_i\sigma_i / \sum_i \sigma_i$. The contribution of the Seebeck coefficient of each band depends on the position of the chemical potential/Fermi level with respect to the band edges ($\eta_{VB} = E_F/(k_BT)$ for the valence band and $\eta_{CB} = (E_F - E_g)/(k_BT)$ for the conduction band) and will be negative for positive band curvature and positive for negative band curvature. We emphasize that the temperature-dependent Seebeck coefficient is much more sensitive towards band structure features compared to the electrical resistivity since energy-independent terms occuring in the numerator and demoninator of the Boltzmann expression, e.g. for the scattering time, get cancelled. Thus, modelling the temperature-dependent Seebeck coefficient allows us to extract band-structure-related parameters, such as the relative position of the Fermi level or band gap. For instance, the slope of $S(T)$ corresponds directly to the position of the Fermi energy, whereas the maximum thermopower S_{max} as well as the temperature of the maximum $T_{S,max}$ are directly linked to the effective band gap. Further details on the modelling procedure may also be found in Refs. [31, 32, 69].

Our parabolic band model takes into account the general features of valence and conduction bands in Fe_2VAl-based compounds. This way, $S(T)$ can be simulated in a broad temperature range. However, since the band structure around E_F of Fe_2VAl-based compounds shows complex features in the reciprocal space, such as non-parabolic bands with varying effective masses in different directions of the Brillouin zone, a quantiative analysis of band parameters such as the band gap is hardly feasible due to the limitations of the model. Moreover, in the presence of antisite disorder the electronic structure near the Fermi energy is expected to change dramatically, as evident from the dramatic changes in the transport properties. Nonetheless, applying the phenomenological parabolic band model to disorder-tuned $Fe_2VAl_{0.9}Si_{0.1}$ qualitatively illustrates the evolution of the electronic structure. Fig. 6 shows the effective energy gaps between the valence band maximum (VBM) and conduction band minimum (CBM), which were obtained by least-squares fitting the temperature-dependent Seebeck coefficient. The transport model suggests a gradual transition towards a more metallic state. The position of the chemical potential, as obtained from the Seebeck coefficient modelling, is for all samples located closer towards the conduction band side, as expected from the excess electron doping due to Al/Si substitution. Therefore, the experimental results presented in this study do not support an enhancement of the Seebeck coefficient

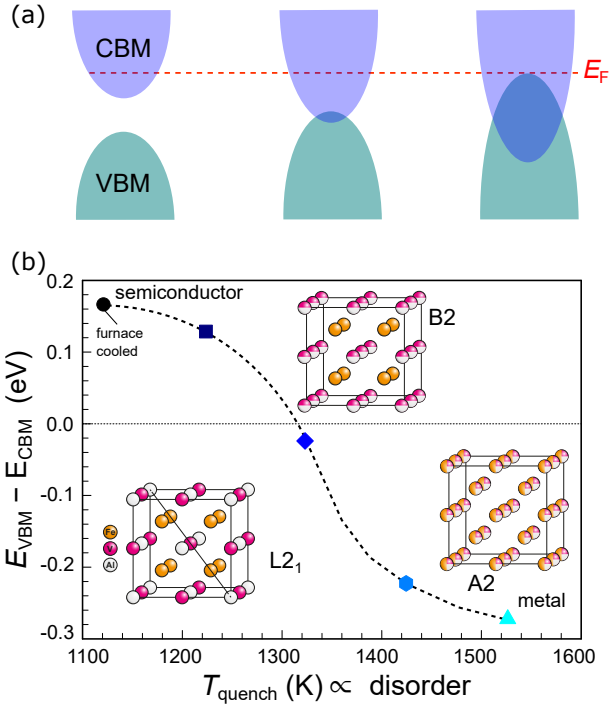

FIG. 6. (a) Sketch of the qualitative evolution of the energy gap between valence band maximum (VBM) and conduction band minimum (CBM) as a function of quenching temperature in disordered $Fe_2VAl_{0.9}Si_{0.1}$ Heusler compounds. For simplification only the two bands around E_F are drawn. It should be noted that absolute values of the gap merely represent an average effective gap extracted from a phenomenological two-band model as described in the text, that may not correspond to the true (pseudo)gap. (b) Evolution of the effective energy gaps from least-squares fitting the temperature-dependent Seebeck coefficient shown as solid lines in Fig. 3. Insets sketch the order – disorder transition in Fe_2VAl-based compounds.

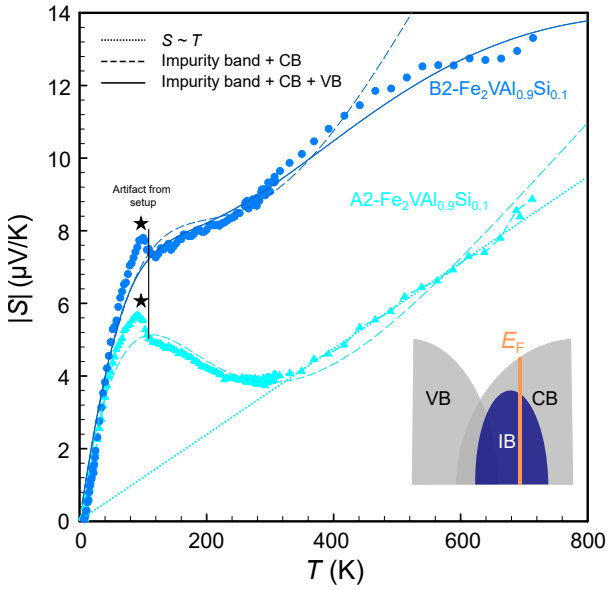

FIG. 7. Low-temperature anomalies in the temperature-dependent Seebeck coefficient of disordered B2- and A2-$Fe_2VAl_{0.9}Si_{0.1}$ Heusler compounds. Dashed and solid lines are least squares fits employing an extended parabolic band model which takes into account a delocalized impurity band with a variable bandwidth W as explained in the text (further details see Ref. [69]). Inset shows schematic of the density of states featuring a valence- and conduction band as well as the impurity band that has been used to model B2-$Fe_2VAl_{0.9}Si_{0.1}$. Due to the metallic nature, only a single parabolic conduction band needs to be included in addition to the impurity band for describing $S(T)$ of A2-$Fe_2VAl_{0.9}Si_{0.1}$ in a broad temperature range. Sharp kinks marked by black stars are most likely an artifact from the measurement setup observed in most of our samples.

and band gap opening driven by antisite defects, as predicted recently [46, 47].

With the help of Monte-Carlo simulations, the occupancy of Fe, V, Al and Si atoms on all sublattices in the $Fe_2VAl_{0.9}Si_{0.1}$ compound can be modelled as a function of temperature. Our calculations show that, even at temperatures far below the B2 – A2 transition, a significant amount of Fe atoms form antisite defects, in agreement with a similar theoretical investigation of stoichiometric Fe_2VAl [48]. Since these defects were shown to lead to in-gap states, a band-gap opening seems unlikely in Fe_2VAl-based samples. Moreover, the predicted band gap opening due to V-Al antisite exchange defects found by Berche *et al.* was calculated for a specific arrangement of the V-Al defects, forming clusters around Fe atoms, since this was shown to be the configuration with the lowest formation enthalpy [46]. However, at high temperatures an entropy contribution to the Gibbs free energy has to be considered $\mathcal{G} = \mathcal{H} - \mathcal{S}T$, with $\mathcal{G}$ being the Gibbs free energy, $\mathcal{H}$ being the free enthalpy and $\mathcal{S}T$ being entropy times temperature, respectively. Since the entropy contribution of V-Al antisite clusters is small compared to a random distribution, this has to be considered as well.

B. Low-temperature Seebeck anomalies

An anomalous low-temperature behavior of the temperature-dependent Seebeck coefficient was found for the disordered $Fe_2VAl_{0.9}Si_{0.1}$ Heusler compounds in their B2 and A2 phases, which is not in line with the linear diffusion term $S \propto T$, often expected for simple metals. As can be seen in Fig. 7, $S(T)$ shows a local maximum around $T = 80\,\mathrm{K}$ for A2-$Fe_2VAl_{0.9}Si_{0.1}$ and only takes on a linear dependence above $\approx 280\,\mathrm{K}$. Similarily, B2-$Fe_2VAl_{0.9}Si_{0.1}$ shows an additional shoulder-like feature roughly at the same temperature. We stress, that corresponding anomalies appear absent in resistivity and magnetization data, ruling out any structural or magnetic transitions. A phonon drag contribution to $S(T)$ seems unlikely in these heavily disordered samples as well. Another enhancement to the Seebeeck coefficient,

in magnetic materials, can arise from spin wave excitations, *i.e.*, the magnon drag effect [45, 70–73]. For a quadratic magnon dispersion, a $T^{3/2}$ dependence of $S(T)$ is expected [73]. However, $S(T)$ cannot be described by such a temperature-dependent behavior either. Such anomalies can also be expected if the eDOS of disordered $Fe_2VAl_{0.9}Si_{0.1}$ strongly deviates or cannot be described by parabolic bands, as a result of the antisite disorder. Thus, $S(T)$ of B2- and A2-$Fe_2VAl_{0.9}Si_{0.1}$ was simulated employing an extended parabolic band model, which takes into account a delocalized impurity band with a bandwidth W. The transport function $\Sigma(E,T)$ in our model is continuously differentiable on both sides of the impurity band and increases monotonically following a power law

$$\Sigma(E,T) = \Sigma_0(T)\left(\frac{E-E_c}{k_B T}\right)^s . \quad (3)$$

Here, E_c represents a critical energy (mobility/transport edge) and $s = 2$ defines the shape of the transport function. Dashed and solid lines in Fig. 7 show that our model is able to trace all the relevant features of $S(T)$ if the impurity bandwidth W is around $100 - 200\,\mathrm{meV}$. However, for structurally ordered $L2_1$-$Fe_2VAl_{0.9}Si_{0.1}$ a mere parabolic band model is sufficient to described $S(T)$ in the whole temperature range.

In summary, low-temperature anomalies of the temperature-dependent Seebeck coefficient $S(T)$ are observed for highly disordered and metallic $Fe_2VAl_{0.9}Si_{0.1}$ which could be ascribed to non-parabolic band structure features and remnants of impurity bands, associated with the antisite disorder. However, a decisive statement on the anomalous $S(T)$ behavior cannot be made since magnetic-field-dependent measurements of the magneto-thermoelectric transport properties are not available and the details of the electronic band structure for these disordered materials is difficult to obtain.

V. CONCLUSION

In conclusion, we investigated the structure – property relationship in disorder-tuned $Fe_2VAl_{0.9}Si_{0.1}$ full-Heusler compounds. Rapid thermal quenching allows systematic tuning of antisite defects across both order – disorder transitions in this compound. Consequently, the partly disordered B2 and even the metastable A2 phase, which so far precluded experimental investigation, can be succesfully realized and analyzed with respect to the thermoelectric and magnetotransport properties. This demonstrates that thermally induced antisite disorder can be utilized as a solid tuning parameter in Fe_2VAl-based compounds and presumably in many other Heusler compounds as well. Experimental results of the temperature-dependent electrical resistivity and Seebeck coefficient in our disorder-tuned samples reveal a gradual transition from a heavily doped semimetal/narrow-gap semiconductor, where the Fermi energy is situated close to the conduction band edge, to a disordered metal. This is further corroborated by a substantial increase in the Hall carrier concentration and decrease of the Hall mobility. Additionally, an anomalous behavior of the Seebeck coefficient as well as a large anomalous Hall effect were observed for fully disordered, metastable A2-$Fe_2VAl_{0.9}Si_{0.1}$. This work provides the first experimental investigation of the electronic transport properties in disorder-tuned Fe_2VAl-based bulk materials within the whole disorder spectrum and shows that temperature-induced antisite disorder can be a tuneable parameter within the family of Heusler compounds.

VI. ACKNOWLEDGEMENTS

Financial support for the research in this paper was granted for F.G., M.P., A.R., E.B. and T.M. by the Japan Science and Technology Agency (JST) programs MIRAI,JPMJMI19A1. A. Prokofiev is acknowledged for assistance with the differential thermal analysis measurement setup. The authors also thank the X-ray center at the TU Wien for their support.

[1] F. Heusler, Verh. Dtsch. Phys. Ges. **5**, 219 (1903).
[2] F. Heusler, W. Starck, and E. Haupt, Verh. Dtsch. Phys. Ges **5**, 219 (1903).
[3] T. Graf, C. Felser, and S. S. Parkin, Progress in solid state chemistry **39**, 1 (2011).
[4] T. Graf, S. S. Parkin, and C. Felser, IEEE Transactions on Magnetics **47**, 367 (2010).
[5] S. Chadov, X. Qi, J. Kübler, G. H. Fecher, C. Felser, and S. C. Zhang, Nature materials **9**, 541 (2010).
[6] M. Jourdan, J. Minár, J. Braun, A. Kronenberg, S. Chadov, B. Balke, A. Gloskovskii, M. Kolbe, H.-J. Elmers, G. Schönhense, *et al.*, Nature communications **5**, 1 (2014).
[7] A. K. Nayak, V. Kumar, T. Ma, P. Werner, E. Pippel, R. Sahoo, F. Damay, U. K. Rößler, C. Felser, and S. S. Parkin, Nature **548**, 561 (2017).
[8] K. Manna, Y. Sun, L. Muechler, J. Kübler, and C. Felser, Nature Reviews Materials **3**, 244 (2018).

[9] F. Aliev, N. Brandt, V. Kozyr'Kov, V. Moshchalkov, R. Skolozdra, Y. V. Stadnyk, and V. Pecharskii, Jetp Lett **45**, 684 (1987).

[10] F. Aliev, N. Brandt, V. Moshchalkov, V. Kozyrkov, R. Skolozdra, and A. Belogorokhov, Zeitschrift für Physik B Condensed Matter **75**, 167 (1989).

[11] H.-H. Xie, J.-L. Mi, L.-P. Hu, N. Lock, M. Chirstensen, C.-G. Fu, B. B. Iversen, X.-B. Zhao, and T.-J. Zhu, CrystEngComm **14**, 4467 (2012).

[12] Y. Kimura and Y.-W. Chai, Jom **67**, 233 (2015).

[13] T. Zhu, C. Fu, H. Xie, Y. Liu, and X. Zhao, Advanced Energy Materials **5**, 1500588 (2015).

[14] H. Xie, H. Wang, C. Fu, Y. Liu, G. J. Snyder, X. Zhao, and T. Zhu, Scientific reports **4**, 1 (2014).

[15] K. S. Kim, Y.-M. Kim, H. Mun, J. Kim, J. Park, A. Y. Borisevich, K. H. Lee, and S. W. Kim, Advanced Materials **29**, 1702091 (2017).

[16] S. Öğüt and K. M. Rabe, Physical Review B **51**, 10443 (1995).

[17] P. Larson, S. Mahanti, and M. Kanatzidis, Physical Review B **62**, 12754 (2000).

[18] G. Y. Yonggang, X. Zhang, and A. Zunger, Physical Review B **95**, 085201 (2017).

[19] B. Ravel, J. O. Cross, M. P. Raphael, V. G. Harris, R. Ramesh, and L. V. Saraf, Applied physics letters **81**, 2812 (2002).

[20] H. C. Kandpal, V. Ksenofontov, M. Wojcik, R. Seshadri, and C. Felser, Journal of Physics D: Applied Physics **40**, 1587 (2007).

[21] Y. Venkateswara, S. Gupta, M. R. Varma, P. Singh, K. Suresh, A. Alam, *et al.*, Physical Review B **92**, 224413 (2015).

[22] Y. Nishino, M. Kato, S. Asano, K. Soda, M. Hayasaki, and U. Mizutani, Physical review letters **79**, 1909 (1997).

[23] R. Weht and W. Pickett, Physical Review B **58**, 6855 (1998).

[24] D. Singh and I. Mazin, Physical Review B **57**, 14352 (1998).

[25] C.-S. Lue, J. H. Ross Jr, C. Chang, and H. Yang, Physical Review B **60**, R13941 (1999).

[26] Y. Nishino, Intermetallics **8**, 1233 (2000).

[27] Y. Nishino, S. Deguchi, and U. Mizutani, Physical Review B **74**, 115115 (2006).

[28] M. Mikami, K. Kobayashi, T. Kawada, K. Kubo, and N. Uchiyama, Journal of Electronic Materials **38**, 1121 (2009).

[29] M. Mikami, Y. Kinemuchi, K. Ozaki, Y. Terazawa, and T. Takeuchi, Journal of Applied Physics **111**, 093710 (2012).

[30] B. Hinterleitner, I. Knapp, M. Poneder, Y. Shi, H. Müller, G. Eguchi, C. Eisenmenger-Sittner, M. Stöger-Pollach, Y. Kakefuda, N. Kawamoto, *et al.*, Nature **576**, 85 (2019).

[31] F. Garmroudi, A. Riss, M. Parzer, N. Reumann, H. Müller, E. Bauer, S. Khmelevskyi, R. Podloucky, T. Mori, K. Tobita, *et al.*, Physical Review B **103**, 085202 (2021).

[32] F. Garmroudi, M. Parzer, A. Riss, N. Reumann, B. Hinterleitner, K. Tobita, Y. Katsura, K. Kimura, T. Mori, and E. Bauer, Acta Materialia **212**, 116867 (2021).

[33] M. Parzer, F. Garmroudi, A. Riss, S. Khmelevskyi, T. Mori, and E. Bauer, Applied Physics Letters **120**, 071901 (2022).

[34] K. Fukuta, K. Tsuchiya, H. Miyazaki, and Y. Nishino, Applied Physics A **128**, 1 (2022).

[35] F. Garmroudi, M. Parzer, A. Riss, S. Beyer, S. Khmelevskyi, T. Mori, M. Reticcioli, and E. Bauer, Materials Today Physics , 100742 (2022).

[36] J. C. Slater, Journal of Applied Physics **8**, 385 (1937).

[37] L. Pauling, Physical Review **54**, 899 (1938).

[38] I. Galanakis, P. Mavropoulos, and P. H. Dederichs, Journal of Physics D: Applied Physics **39**, 765 (2006).

[39] S. Skaftouros, K. Özdoğan, E. Şaşıoğlu, and I. Galanakis, Physical Review B **87**, 024420 (2013).

[40] H. Okamura, J. Kawahara, T. Nanba, S. Kimura, K. Soda, U. Mizutani, Y. Nishino, M. Kato, I. Shimoyama, H. Miura, *et al.*, Physical review letters **84**, 3674 (2000).

[41] S. Anand, R. Gurunathan, T. Soldi, L. Borgsmiller, R. Orenstein, and G. J. Snyder, Journal of Materials Chemistry C **8**, 10174 (2020).

[42] B. Hinterleitner, F. Garmroudi, N. Reumann, T. Mori, E. Bauer, and R. Podloucky, Journal of Materials Chemistry C (2020).

[43] S. Maier, S. Denis, S. Adam, J.-C. Crivello, J.-M. Joubert, and E. Alleno, Acta Materialia **121**, 126 (2016).

[44] E. Alleno, A. Berche, J.-C. Crivello, A. Diack-Rasselio, and P. Jund, Physical Chemistry Chemical Physics **22**, 22549 (2020).

[45] H. Matsuura, M. Ogata, T. Mori, and E. Bauer, Physical Review B **104**, 214421 (2021).

[46] A. Berche, M. T. Noutack, M.-L. Doublet, and P. Jund, Materials Today Physics **13**, 100203 (2020).

[47] J. C. A. do Nascimento, A. Kerrigan, P. Hasnip, and V. K. Lazarov, Materials Today Communications , 103510 (2022).

[48] F. Garmroudi, M. Parzer, A. Riss, A. V. Ruban, S. Khmelevskyi, M. Reticcioli, M. Knopf, H. Michor, A. Pustogow, T. Mori, *et al.*, Nature Communications **13**, 1 (2022).

[49] F. Ducastelle and F. Gautier, Journal of Physics F: Metal Physics **6**, 2039 (1976).

[50] A. V. Ruban, S. Shallcross, S. Simak, and H. L. Skriver, Physical review B **70**, 125115 (2004).

[51] L. Vitos, I. Abrikosov, and B. Johansson, Physical review letters **87**, 156401 (2001).

[52] C.-S. Lue, J. H. Ross Jr, K. Rathnayaka, D. Naugle, S. Wu, and W. Li, Journal of Physics: Condensed Matter **13**, 1585 (2001).

[53] Y. Feng, J. Rhee, T. Wiener, D. W. Lynch, B. Hubbard, A. Sievers, D. L. Schlagel, T. A. Lograsso, and L. Miller, Physical Review B **63**, 165109 (2001).

[54] Y. Nishino, H. Sumi, and U. Mizutani, Physical Review B **71**, 094425 (2005).

[55] B. Suh, S. Baek, and J. Rhee, Journal of the Korean Physical Society **48**, 288 (2006).

[56] M. Vasundhara, V. Srinivas, and V. Rao, Physical Review B **78**, 064401 (2008).

[57] S. Bandaru and P. Jund, physica status solidi (b) **254**, 1600441 (2017).

[58] A. Berche and P. Jund, Computational Materials Science **149**, 28 (2018).

[59] C. Van der Rest, A. Schmitz, and P. J. Jacques, Acta Materialia **142**, 193 (2018).

[60] G. Botton, Y. Nishino, and C. Humphreys, Intermetallics **8**, 1209 (2000).

[61] M. Jamer, B. Assaf, G. Sterbinsky, D. Arena, L. Lewis, A. Saúl, G. Radtke, and D. Heiman, Physical Review B **91**, 094409 (2015).
[62] I. Knapp, B. Budinska, D. Milosavljevic, P. Heinrich, S. Khmelevskyi, R. Moser, R. Podloucky, P. Prenninger, and E. Bauer, Physical Review B **96**, 045204 (2017).
[63] B. Hinterleitner, P. Fuchs, J. Rehak, F. Garmroudi, M. Parzer, M. Waas, R. Svagera, S. Steiner, M. Kishimoto, R. Moser, *et al.*, Physical Review B **102**, 075117 (2020).
[64] C. S. Lue, C. Chen, J. Lin, Y. Yu, and Y. Kuo, Physical Review B **75**, 064204 (2007).
[65] M. Vasundhara, V. Srinivas, and V. Rao, Physical Review B **77**, 224415 (2008).
[66] D. I. Bilc and P. Ghosez, Physical Review B **83**, 205204 (2011).
[67] N. Tsujii, A. Nishide, J. Hayakawa, and T. Mori, Science advances **5**, eaat5935 (2019).
[68] N. Manyala, Y. Sidis, J. F. DiTusa, G. Aeppli, D. P. Young, and Z. Fisk, Nature materials **3**, 255 (2004).
[69] G. Rogl, F. Garmroudi, A. Riss, X. Yan, J. Sereni, E. Bauer, and P. Rogl, Intermetallics **146**, 107567 (2022).
[70] F. Blatt, D. Flood, V. Rowe, P. Schroeder, and J. Cox, Physical Review Letters **18**, 395 (1967).
[71] M. Lucassen, C. Wong, R. Duine, and Y. Tserkovnyak, Applied Physics Letters **99**, 262506 (2011).
[72] B. Flebus, R. A. Duine, and Y. Tserkovnyak, EPL (Europhysics Letters) **115**, 57004 (2016).
[73] S. J. Watzman, R. A. Duine, Y. Tserkovnyak, S. R. Boona, H. Jin, A. Prakash, Y. Zheng, and J. P. Heremans, Physical Review B **94**, 144407 (2016).